RESEARCH ARTICLE

Engineering
in Life Sciences

Developing a surface acoustic wave-induced microfluidic cell lysis device for point-of-care DNA amplification

Abbas Ali Husseini[1] 🟢 | **Ali Mohammad Yazdani**[2,3] | **Fatemeh Ghadiri**[1,4] | **Alper Şişman**[5,6,7]

[1]Life Science and Biomedical Engineering Application and Research Center, Istanbul Gelisim University, Istanbul, Turkey

[2]Mechanical Engineering Program, Faculty of Engineering, Marmara University, Istanbul, Turkey

[3]Machine Program, Vocational School, Nişantaşı University, Istanbul, Turkey

[4]Department of Computer Engineering, Istanbul University Cerrahpaşa, Istanbul, Turkey

[5]Electrical and Electronics Engineering Program, Faculty of Engineering, Marmara University, Istanbul, Turkey

[6]Sabanci University Nanotechnology and Application Center (SUNUM), Sabanci University, Istanbul, Turkey

[7]Faculty of Electrical Engineering, Mathematics and Computer Science, Delft University of Technology, Delft, The Netherlands

Correspondence
Alper Şişman, Electrical and Electronics Engineering Program, Faculty of Engineering, Marmara University, Istanbul, 34722, Turkey.
Email: alper.sisman@marmara.edu.tr

Abstract

We developed a microchip device using surface acoustic waves (SAW) and sharp-edge glass microparticles to rapidly lyse low-level cell samples. This microchip features a 13-finger pair interdigital transducer (IDT) with a 30-degree focused angle, creating high-intensity acoustic beams converging 6 mm away at a 16 MHz frequency. Cell lysis is achieved through centrifugal forces acting on *Candida albicans* cells and glass particles within the focal area. To optimize this SAW-induced streaming, we conducted 42 pilot experiments, varying electrical power, droplet volume, glass particle size, concentration, and lysis time, resulting in optimal conditions: an electrical signal of 2.5 W, a 20 μL sample volume, glass particle size below 10 μm, concentration of 0.2 μg, and a 5-min lysis period. We successfully amplified DNA target fragments directly from the lysate, demonstrating an efficient microchip-based cell lysis method. When combined with an isothermal amplification technique, this technology holds promise for rapid point-of-care (POC) applications.

KEYWORDS
cell lysis, droplet, micro-glass particle, surface acoustic wave

1 | INTRODUCTION

Cell lysis represents a pivotal initial step in the majority of omics analyses, entailing the disruption of the cell membrane and the subsequent release of its contents via the application of an external force [1]. An effective cell lysis methodology, coupled with a streamlined downstream analysis, remains indispensable in ensuring the attainment of precise and accurate results [1]. In general, conventional cell lysis methods can be classified into two categories: mechanical and non-mechanical techniques. Mechanical lysis relies upon shear forces generated either by high pressure or bead beating to rupture the cell membrane and release intracellular components [2, 3]. High-pressure mechanical lysis is typically achieved by directing a large-scale cell suspension through an orifice valve, thereby inducing membrane rupture [4]. Conversely, bead beating leverages solid beads composed of materials such as glass, zirconium oxide, tungsten carbide, stainless steel, or ceramics to generate shear forces through solid-solid interactions, facilitating laboratory-scale lysis [5]. Non-mechanical approaches encompass the utilization of physical methods, chemical chaotropic agents, or enzymatic digestion to disrupt the cell membrane [3, 5, 6]. Conventional techniques excel in handling large sample volumes, scalability, and cost-effectiveness for high-throughput operations but may be less suitable for certain specialized (single cell, low volume sample and so on) or point-of-care (POC) applications due to dependence on well-equipped laboratories and sample size. Microchip-based cell lysis devices offer advantages and overcoming the limitations and incompatibilities of conventional approaches in terms of portability, speed, and sample size compatibility, making them ideal for POC applications where rapid and gentle cell lysis is crucial [3, 7, 8].

Microfluidic lysis technology leverages established conventional approaches at the microscale, including well-known mechanical and non-mechanical methods [3, 7]. For instance, several microchip-based devices employ shear forces generated by bead beating or friction using nanoscale barbs to mechanically disrupt cells [3, 7, 9]. Thermal lysis presents an attractive option due to the ease of integrating polymerase chain reaction (PCR) modules into microfluidic devices [3, 7]. While chemical lysis in chip devices may present challenges, such as complex injection channel structures, reagent delivery time, and post-lysis washing steps, these chemical lysis-based chips offer substantial systems capable of achieving high-throughput lysis, thereby reducing processing time and manual labor [10–12]. Additionally, chip-based devices have the potential to employ high-energy sound waves,

PRACTICAL APPLICATION

The study's conclusions include a very effective microchip-based cell lysis technique that uses sharp-edged glass microparticles and SAW to quickly lyse low concentrations of cell samples. The creation of a portable point-of-care DNA testing equipment is practically possible with this technique. The tool would make it possible to quickly and accurately test DNA in a variety of locations, including rural areas, clinics, hospitals, and even non-traditional healthcare settings.

strong electric fields, lasers, and optically induced dielectrophoretic techniques [3].

Surface acoustic waves (SAWs), which are nanometer-order amplitude traveling waves propagating on the surface of a piezoelectric crystal substrate via an interdigital transducer (IDT) driven by an electrical signal, can be integrated into microfluidic devices, enabling potentially less complex operations [9, 13, 14]. Several significant advancements have been made in the field of cell lysis, with diverse approaches and SAW technologies. One noteworthy advancement involves the application of Traveling Surface Acoustic Waves (TSAW) for the concurrent encapsulation and lysis of specific cells, thereby facilitating the subsequent analysis of individual cellular omics [15]. An additional study has introduced an additive-free methodology employing TSAW in conjunction with a microfluidic device for bacterial lysis and the extraction of nucleic acids and proteins. This lysis process occurs within microchannels, processing 1 mL or 2×10^9 cells per hour, utilizing a TSAW frequency of 13 MHz and a power level of 15.8 W [16]. It is pertinent to note that the utilization of higher power levels poses a risk of inducing cracks in the piezoelectric substrate, and the method is unsuitable for applications with lower sample volumes. In a different research endeavor aimed at the lysis of Gram-positive bacterium *Geobacillus thermoglucosidasius*, the compact dimensions of Surface Acoustic Wave (SAW) devices were found to be advantageous for potential POC instrumentation. However, this study encountered a limitation with regards to its lysis efficiency, which was measured at 21% [17]. Lastly, a study employed high-speed stream collision induced by SAW within droplets for efficient POC cell lysis. The lysis process achieved a remarkable efficiency exceeding 95% when utilizing 6.3 W of power, accomplishing cell lysis within a brief timeframe of 20 s. The design incorporated micropillars with sharp edges within the lysis

chamber. However, the lysis efficiency in the absence of micropillars was found to be less than 20%. It is estimated that the streaming velocity is about 10–20 cm/s at an RF power of 4 W and it may decrease slightly due to the existence of micro-pillars [18]. This probably affects the efficiency of the lysis at a lower power level required to increase the electrical signal.

While previous research has explored various microchip-based cell lysis techniques using SAWs, some limitations, such as lysis efficiency and suitability for low sample volumes, have been identified. Therefore, there is a need for further investigation into the development and optimization of microchip devices that can efficiently perform cell lysis on small sample volumes, addressing the challenges associated with POC applications. The objective of this study is to develop a novel microchip device that utilizes focused surface acoustic waves and irregular sharp-edge glass microparticles for rapid lysis of low-volume samples, with the aim of enabling POC-lysis applications.

2 | THEORETICAL FRAMEWORK

2.1 | Mechanical cell lysis

A wide array of mechanical and non-mechanical techniques has been developed for cell lysis, applicable at both macro and micro scales. Mechanical lysis methods rely on the application of shear forces to disrupt the cell membrane and are widely embraced due to their combination of high throughput and efficient lysis. Among these methods, the bead mill technique is extensively employed in laboratory-scale mechanical cell lysis. Cell disruption primarily occurs through shear forces generated by the rotational movement of cells in the presence of beads, resulting in cell grinding. Several factors influence the efficiency of this process, including bead diameter and density, cell concentration, and agitator speed [2, 6]. In the proposed method, irregular sharp-edge glass particles are employed instead of conventional beads. While there are similarities between the proposed cell lysis using micro-glass particles and the well-known bead-beating method, significant differences exist. The bead-beating method operates based on the principle of applying vertical pressure to the cell, sandwiched between the bead and a fixed surface, leading to cell disruption. In contrast, the sharp glass microparticles used in our method exert shear forces on the cell wall as the cell rubs against these particles, ultimately causing cell disintegration. The absence of sharp edges in the beads used in the conventional method makes cell lysis more challenging in comparison.
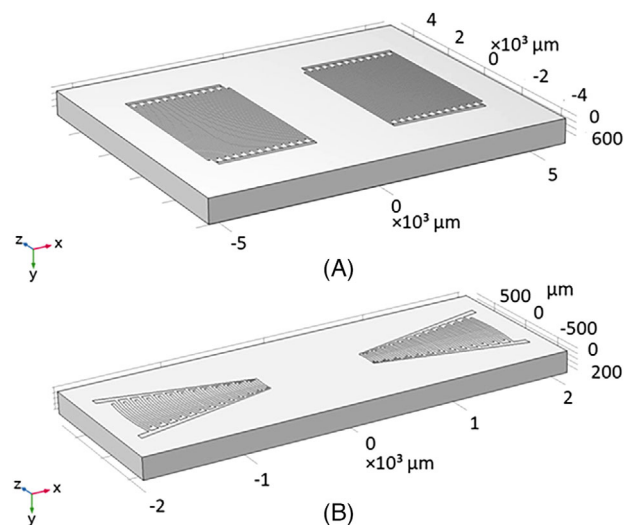

FIGURE 1 IDT structure and design parameters, (A) regular IDT structure, (B) focused IDT [30].

2.2 | Traveling surface acoustic wave (TSAW)

The Rayleigh surface acoustic wave mode (R-SAW) is a longitudinally and vertically polarized wave that propagates along the surface of an elastomeric material, exhibiting an exponentially decaying amplitude with depth [19, 20]. In microfluidic systems, R-SAWs are typically generated on a piezoelectric substrate, such as quartz or lithium niobate, with IDTs patterned on the surface [21]. The primary function of the IDTs is to convert an electrical radio frequency (RF) signal into mechanical vibrations, thereby enabling the generation of periodically dispersed mechanical forces and vice versa [21, 22]. A SAW device commonly consists of either a single IDT (one-port device) or two reciprocally patterned IDTs (two-port device) in a regular or focused configuration on a piezoelectric wafer (Figure 1). SAW devices with two IDTs find utility in sensor systems or for actuators that utilize standing SAW [23]. Conversely, TSAW devices typically employ a single IDT, primarily serving as an actuator for particle separation/mixing applications and droplet manipulation [13].

For effective actuation, TSAW devices generate transverse waves that transition to the longitudinal mode when the medium changes from solid to liquid [24, 25]. This longitudinal wave induces acoustic streaming within the liquid, creating non-contact motion. Two fundamental forces contribute to the motion within the fluid: the acoustic radiation force (ARF) and the acoustic streaming force (ASF). The surface vibrations of TSAW generate a wave that propagates in the liquid, giving rise to a pressure field known as the ARF. The energy carried by the wave results

in a streaming phenomenon that exerts a force, known as the ASF, on the particles within the fluid. The frequency of TSAW determines the characteristics of the ARF, while the mechanical properties of the fluid influence the ASF [26]. The ARF is given by expression (1), where F^{rad}, a, p_0, p_{in} and v_{in} represents radiation force, particle radius, compressibility of the liquid and pressure and velocity of the incoming wave respectively [27]. The reflection coefficients f_1 and f_2 are given by (2), where κ_p, κ_0, ρ_p, and ρ_0 show compressibility and density for particle and liquid [27]. The ASF (F^{drag}) is the function of viscosity of the liquid (μ), particle radius(a), and the velocity difference between the acoustic stream (v_{stream}) and the particle (v_p) (3) [27].

$$F^{rad} = -\frac{4\pi}{3}a^3 \nabla \left[\frac{1}{2}Re[f_1]\kappa_0 \langle p_{in}^2 \rangle - \frac{3}{4}Re[f_2].\rho_0.\langle v_{in}^2 \rangle \right]$$

(1)

$$f_1 = 1 - \frac{\kappa_p}{\kappa_0}, \quad f_2 = \frac{2\left(\frac{\rho_p}{\rho_0} - 1\right)}{2\left(\frac{\rho_p}{\rho_0}\right) + 1}$$

(2)

$$F^{drag} = 6\pi\mu a \left(\langle v_{stream} \rangle - v_p \right)$$

(3)

Therefore, the motion of the particles in the droplet under the effect of traveling surface acoustic waves can be described using Newton's second law (4) [28].

$$m_p \frac{dv_p}{dt} = F^{rad} + F^{drag}$$

(4)

where m_p is the mass of the particle.

2.3 | TSAW device

An IDT comprises a pair of metallic structures shaped like combs, arranged in an intertwined fashion (Figure 1). The distance between the centers of two consecutive IDT fingers within the same comb structure corresponds to the wavelength of the surface acoustic wave (SAW), while the ratio of the finger width to half of the wavelength ($\lambda/2$) is defined as the metallization ratio. If the finger width value is $\lambda/4$, the metallization ratio is 0.5. The number of finger pairs in the IDT and the aperture geometry collectively determine the bandwidth and directivity of the generated SAW [22].

In contrast, when SAWs propagate in a piezoelectric substrate and interact with the adjacent fluid, they undergo refraction at the liquid-substrate interface due to differences in sound velocity. Consequently, the SAW, originally a transverse wave in the substrate, transforms into a longitudinal wave in the liquid medium. The longitudinal waves give rise to significant inertial forces and fluid velocity, resulting in the formation of acoustic streams within the droplet and facilitating mixing processes [24, 25]. The streaming pattern induced by SAWs is influenced by various factors, including the geometry of the confined liquid, as well as the incident position, angle, and operating frequency of the SAW [29].

3 | MATERIAL AND METHODS

This study proposes an innovative on-chip method for low-volume cell lysis by integrating a surface acoustic wave (SAW)-based approach with irregular sharp-edge micro-glass particles. The high-efficiency disruption of cells within a droplet is achieved using a focused T-SAW microchip. To accomplish this, a cell suspension containing an optimized concentration of irregular sharp-edge micro-glass particles is introduced to the focal point of the designed focused T-SAW microchip (Figure 2A). The T-SAW generates two primary forces within the droplet: the acoustic streaming force (ASF) and the ARF, resulting in the rapid radial motion of particles inside the droplet (Figure 2B). However, the speed of cells and micro-glass particles may differ due to variations in their weight and density. Consequently, when the faster-moving cells collide with the irregular sharp-edge glass particles (Figure 2C), the lateral forces applied by the particles cause the membranes of the cells to rupture.

3.1 | Design of the cell lysis chip

The cell lysis chip utilizes Transverse Surface Acoustic Waves (TSAWs) to transmit acoustic energy into a droplet containing a mixture of irregular glass particles and cells intended for lysis. The TSAW is generated by a single focused Interdigital Transducer (F-IDT) electrode, which emits high-intensity acoustic waves targeted at its focal region. By placing the droplet precisely at the focal region of the F-IDT, an efficient lysis process is achieved. The device is specifically designed to operate at a theoretical frequency of 16 MHz, enabling excitation of Rayleigh waves with a wavelength of 250 μm on the LiNbO$_3$ substrate. With the given parameters, the dimensions of the device are 10 mm $\times$ 10 mm. The focus angle of the F-IDT is determined through simulation studies optimized using COMSOL Multiphysics [31]. The F-IDT consists of 13 pairs of fingers, while the focus angle of the IDT is set at
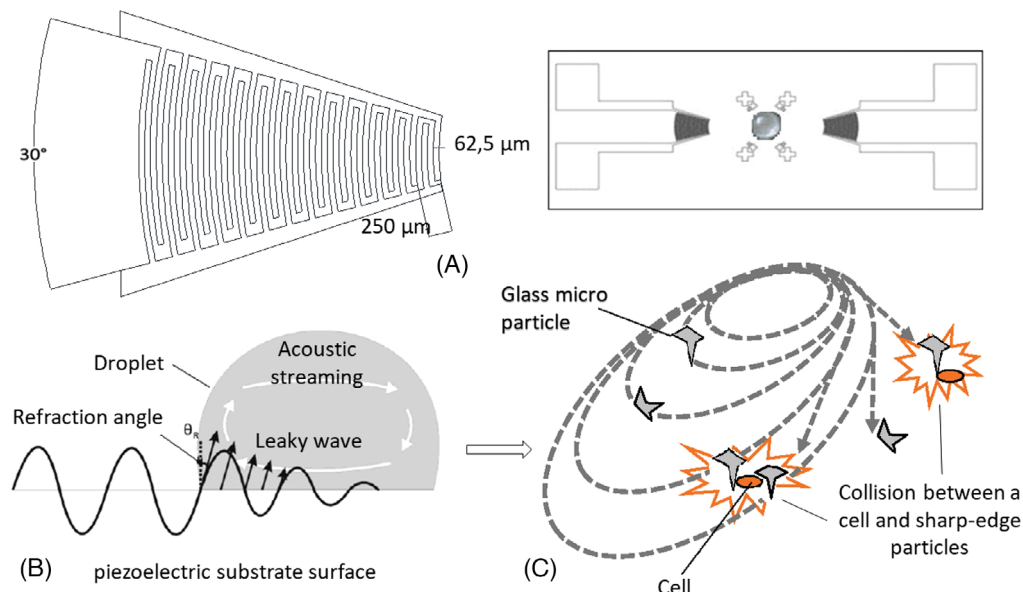
FIGURE 2 Cell lysis principle of surface acoustic wave-based approach using sharp-edge irregulated micro-glass particles: (A) Schematic of focused IDT and device design. (B) The longitudinal wave causes acoustic streams within the droplet, creating a non-contact motion in a radial direction at high speed. (C) Collision between cells and sharp-edge glass micro particles inside the droplet causing cell lysis.

30°, resulting in a focal distance of 6 mm. The metallization ratio for the IDT design is 50%, corresponding to an IDT-finger width of 62.5 μm (Figure 2A).

3.2 | Device fabrication

The fabrication of the cell lysis chip employs a single lithography stage followed by a wet etching process. The fabrication steps are: (1) The fabrication of the cell lysis chip employs a single lithography stage followed by a wet etching process. (2) The 500 μm thickness-wafer, (128o-Y Cut, X propagation LiNbO$_3$ substrate) was cleaned in an acetone bath (in ultrasound cleaner) for 10 min. Then it was rinsed with isopropanol and deionized water. Nitrogen spray gun was used to dry the sample. (3) The Chromium metal film was sputtered on the substrate wafer (NVHP-400: NANOVAK, Ankara, Turkey). DC-Sputtering for 15 min at 500 mA constant current was used to deposit 250 nm Chromium. (4). A positive photoresist AZ5214E (Merck, Kenil-worth, NJ) was spun on the wafer for 35 s at 4000 rpm to have 1 μm thickness. (5) The wafer was then soft-baked at 110°C for 50 s before ultraviolet (UV) exposure. (6) The wafer was exposed to UV light with 20 W/m^2 intensity for 7 s to transfer the IDT patterns from the mask. (7) The exposed wafer was then developed in the developer solution AZ 726MIF (Merck, Kenilworth, NJ) for 35 s to remove the exposed photoresist from the surface. (8) The features were formed by wet-etching of the

chromium using the etchant Cr01 (Microchems, Austin, TX). (9) The remaining photoresist was removed in an acetone bath. The wafer was then diced using a pen scriber (Figure 3).

3.3 | Production of sterile glass microparticles

In the cell disruption stage, sterile glass microparticles were utilized. These particles were produced in different micro sizes. The glass pieces were first washed and sterilized with sterile water and propanol alcohol before being used to make micro-glass particles. The glass pieces were ground in a ring-pulverizer for 5 min after the propanol alcohol was entirely evaporated. The product was then sifted for 20 min using a multi-tray (125, 75, 45, and 38 μm mesh) vibrating sieve shaker with a 90-oscillation rate. The collected powder between 45 and 38 μm sieve trays was rinsed with propanol alcohol to eliminate small particles before being dried and weighed as 40-micron particles. The powder, which was then collected under a 38-micron sieve, was applied to further wet grinding via a planetary mono mill with four silicon nitride balls (5 mm diameter) in a silicon nitride bowl using propanol as the dispersing liquid. A rotary evaporator was then used to dry the slurry. Later, a sonication bath was used to collect the dried product, which was then sized using a particle size analyzer (Mastersizer 2000, Malvern, UK).
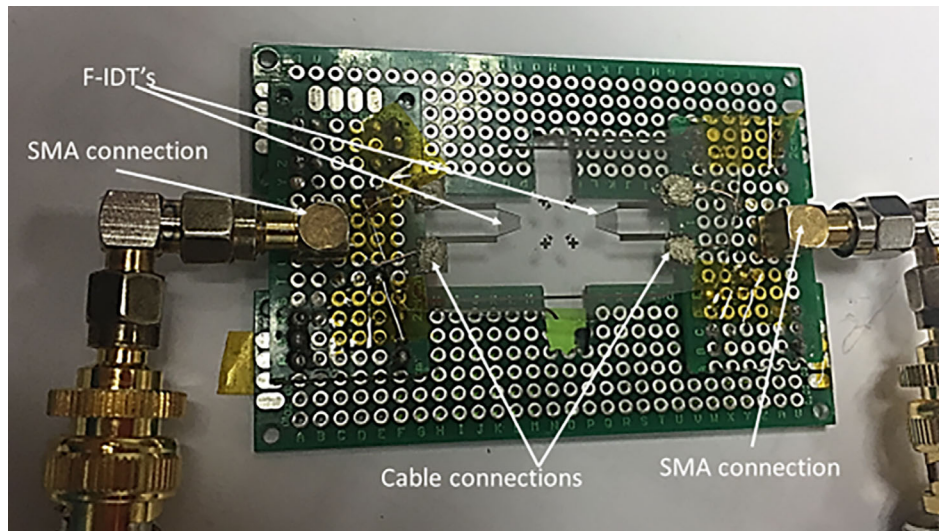
Engineering
in Life Sciences

FIGURE 3 Fabricated actuator.

3.4 | Experimental studies

3.4.1 | Actuator electrical characterization

The electrical measurements provide direct insights into the optimal operating frequency of the actuator. In the case of a one-port device, the s11 parameter can indicate the resonance frequency, which corresponds to the minimum reflection. In this study, a vector network analyzer (Copper Mountain, Indianapolis, USA) was employed to determine the s11 parameter as a function of frequency. The frequency response of the designed actuator was measured, revealing resonant peaks indicative of Rayleigh waves at 15.484 MHz, with a return loss of approximately −1.1 dB (Figure 4). The observed low return loss value suggests an impedance mismatch near the resonance frequency. The S11 measurement was repeated multiple times over an extended duration, demonstrating consistent results. Therefore, the SAW resonator fulfills the requirements for the intended actuation application.
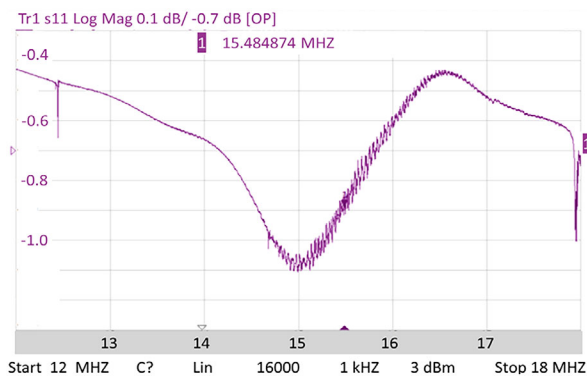

FIGURE 4 The resonance frequency analysis of the designed chip using a vector network analyzer (Copper Mountain, Indianapolis, USA).

3.4.2 | Experimental setup

The actuator is stimulated by a sinusoidal signal at its resonance frequency, which is generated by an RF signal generator (Aim-TTi Inc., Cambridge-shire, UK). This continuous wave sine signal is then amplified using a wideband RF amplifier (Acquitek, Massy, France) with a gain of 47 dB. The amplified signal is applied to the actuator through a wattmeter (Bird Electronic Corp., Cleveland, USA), capable of measuring both transmitted and reflected power (refer to Figure 5). The surface of the chip, particularly the focal area, is observed using a microscope (Leica, Wetzlar, Germany) to monitor the actuation process.

The experimental procedure involves placing a droplet containing a specific concentration of cells and microparticles onto the focal area of the device. By applying a sinusoidal signal at the resonance frequency to the IDT, the device generates Rayleigh surface acoustic waves (R-SAW) in the form of mechanical stress propagating on the LiNbO$_3$ surface. Subsequently, a traveling SAW propagates into the liquid within the droplet, resulting in

FIGURE 5 Experimental setup.

an attenuated acoustic wave. This wave induces acoustic streaming within the droplet, leading to the transportation of cells and microparticles along the streaming flow. The rapid rotation of cells colliding with the sharp edges of particles generates high shear forces, which can mechanically lyse the cells. The structure of the actuator and the experimental setup are depicted in Figures 2A and 5, respectively. Additionally, a visual demonstration of the induced acoustic streaming on the microchip can be found in supplementary video document 1.

3.4.3 | Cell culture preparation

The chosen cell line for evaluating the lysis performance of the acoustofluidic device was Candida albicans strain SC 5314. These cells were cultured in yeast extract peptone dextrose culture media, which we prepared in-house using the following components: 20 g (2%) glucose, 20 g (2%) peptone, and 10 g (1%) yeast extract. We adjusted the volume to 1 L using deionized water. For solid medium preparation, we added 20 g (2%) agar to the media and sterilized it through autoclaving. The cells were cultured overnight in a solid medium at 37°C in an incubator.

Before conducting the experiments, we prepared pre-experiment suspensions of Candida cells in Phosphate-buffered saline. We created the saline solution in-house by dissolving 8 g of NaCl, 0.2 g of KCl, 1.44 g of Na2HPO4, and 0.24 g of KH2PO4 in 800 mL of distilled water. We adjusted the pH and volume of the solution to 7.4 using HCl and a total volume of 1 L of distilled water, respectively. The solution was then autoclaved.

To prepare the cell suspensions for the experiments, we harvested cells from colonies grown on the solid medium and suspended them in 1 mL of Phosphate-buffered saline. Various suspensions of cells were prepared, and we determined the cell concentration per 1 mm³ by counting the cells under a microscope using a Thoma chamber just before the experiments.

Each cell suspension was then combined with specific glass micro-particle sizes ($\leq$10–150 μm) and particle concentrations (0.1–0.3 μg/mL), and gently mixed.

3.4.4 | Parameter optimization for efficient cell lysis

The induction of acoustic streaming for particle movement within the droplet was investigated by varying the RF driving power from 30 dBm to 37 dBm at the resonance frequency. The flow rate of the acoustic stream was visualized using Fluoresbrite® YG microspheres with a diameter of 10.0 μm, observed under a fluorescence micro-

TABLE 1 Biotin and FITC labeled Loop-mediated isothermal amplification primers design.

Primer	Label	Sequence
Forward	Biotin	ATGTTCCAGCTTTCTACGT
Backward	FITC	AGTGAAACTGTAACACGT
Forward inner	Biotin	CACCAGAATCCAAAACAATACC-GGCCATTCAGCTGTTTTGTCTT
Backward inner	FITC	GTTGTTCCAATTTACGCTGGTTTC-CAAATGGTTGGTCAAGTCTC

scope (Leica Microsystems) (see supplementary video document 1).

To optimize the parameters for achieving high cell lysis efficiency, a pilot experiment was conducted involving 42 different combinations of specific ranges for electrical power (1–5 W), droplet volume (10–30 μL), glass micro-particle size ($\leq$10–150 μm), particle concentration (0.1–0.3 μg/mL), and lysis time (1–5 min). The lysis efficiency was calculated as the percentage of disrupted cells among all cells observed in the bright field under a 40× objective. A regression analysis was employed to assess the impact of each parameter on the lysis efficiency.

Subsequently, a machine learning regression model was applied to predict the optimal combination of parameters for highly efficient lysis. The model was trained using the parameters from the 42 experimental conditions and tested with 394 new parameter combinations to predict the optimal conditions that would result in over 90% cell lysis efficiency. These optimal conditions were then experimentally verified to determine the best operating condition for the designed chip's performance.

3.5 | Downstream analysis for cell lysis

3.5.1 | Loop-mediated isothermal amplification (LAMP)

The lysed samples were collected and subsequently centrifuged at 5500 rpm for 10 min to remove cell debris and microparticles. Then, the supernatant was collected for the direct amplification of a 250 bp fragment of the actin (act1) gene using a specific Biotin and FITC labeled LAMP primer (Table 1). The LAMP reaction was prepared according to the recommendations of New England Biolabs with the WarmStart LAMP kit, with a total reaction volume of 25 μL (12.5 μL ready-to-use 2× LAMP Master Mix, 2.5 μL 10× primer mixture, and 5 μL target DNA from the lysate). LAMP reactions were carried out at 65°C using a thermal cycler.

3.5.2 | Loop-mediated isothermal amplification (LAMP)

Fluorometric analysis

To visualize the amplification, 0.5 μL of a 50x LAMP fluorescent dye was added to the reaction vessel, following the instructions provided by NEB (USA). The fluorescent emission level was measured using a Fluo-100 Alshungh fluorometry device (Hangzhou Allsheng instrument, PRC) with blue wavelengths set at 460 nm. Additionally, the appearance of white turbidity in the reaction fluid, indicative of DNA amplification, was observed visually under daylight conditions. The concentration of nucleic acid was also measured in the final reaction vessel.

Lateral flow test

The Milenia HybriDetect1 lateral flow test, designed to detect amplicons labeled with biotin and FITC (or FAM), along with primers containing these entities, was used to detect the LAMP amplicons. The sample pad contained gold-labeled anti-FITC antibodies, while the test and control lines were coated with biotin-ligands and anti-rabbit antibodies, respectively. When the double-labeled amplicons (FITC and biotin) diffused through the chromatographic membrane, the amplicons were captured by the biotin-ligands at the 5′ ends, resulting in their appearance at the test line. Simultaneously, gold-labeled anti-FITC antibodies bound to FITC at the 3′ ends, producing a red-pink color. Non-captured gold-labeled anti-FITC antibodies were immobilized at the control line by anti-rabbit antibodies. The appearance of color only at the control line indicated the absence of the target amplicons.

4 | RESULTS AND DISCUSSION

4.1 | Glass microparticles size analysis

After pulverization, the glass fragments were sorted into different size categories based on their dimensions. Particle size analysis was conducted to determine the size distribution across four distinct categories: <10 μm, 10–50 μm, 50–100 μm, and 100–150 μm (as depicted in Figure 6A). The most uniform particle size was observed in the category of particles <10 μm in size. Figure 6B illustrates the size distribution and cumulative relative frequency of glass microparticles, with an approximate size of 10 μm, as determined by the particle size analyzer. The particle size range fell between 1.3 and 52.5 μm, with an average size of 10 μm. Approximately 55% of the particles were found to be smaller than 10 μm in size.

4.2 | Optimization results

Candida albicans strain SC 5314 was chosen as the model cell to demonstrate the superior efficiency of the new lysis method compared to the conventional approach. Several key independent variables were identified as significant factors influencing cell lysis efficiency, including the electrical input power applied to IDTs, droplet volume for high-throughput lysis, glass microparticle size, particle concentration, and process duration.

The statistical analysis of the experimental data involved a multiple regression analysis, yielding pertinent regression parameters. Notably, the computed values included a multiple correlation coefficient (R) of 0.9, an R-squared coefficient (R^2) of 0.8, an adjusted R-squared coefficient of 0.7, and a standard error of 0.1. These outcomes collectively reflect the model's robust overall fit, underscored by the notably high values of both R and R^2, signifying the model's capacity to elucidate a substantial portion of the variability inherent to lysis efficiency.

However, the adjusted R-squared coefficient serves to temper this appraisal by considering the complexity of the model, thereby intimating potential factor for further refinement or the inclusion of additional pertinent variables. Meanwhile, the low standard error is indicative of the model's predictive precision, suggesting its utility as a means of forecasting optimal conditions for cell lysis, obviating the necessity for extensive experimental trials.

Notably, glass microparticle size (p-value < 0.0001), lysis time (p-value <0.0001), and droplet volume (p-value = 0.0004) emerged as the most critical parameters affecting lysis efficiency in the current design. An electrical power range of 1.5–4.5 W was suggested to induce streams in droplets, with optimal lysis observed at 2.5 W. Supplementary video 2 demonstrates the stream velocity under 2.5 W. However, it should be noted that higher input power is associated with increased temperature on the piezoelectric substrate, leading to droplet evaporation, degradation of biological materials, and material loss, posing a challenge in the current design. Nonetheless, the heating induced by SAW propagation within the sample holds the potential for implementing thermal cycling for PCR on the same platform if appropriately designed [32].

While SAW-assisted thermal-based cell lysis technology in PDMS microchannels has proven suitable for continuous cell lysis, particularly for larger volume samples, the current device prioritizes droplet samples, making it ideal for handling volume-limited samples at the point of care. In this design, optimal lysis was achieved with a 20 μL droplet volume. However, working with lower volumes presented challenges such as early evaporation before completion of lysis and difficulties in harvesting
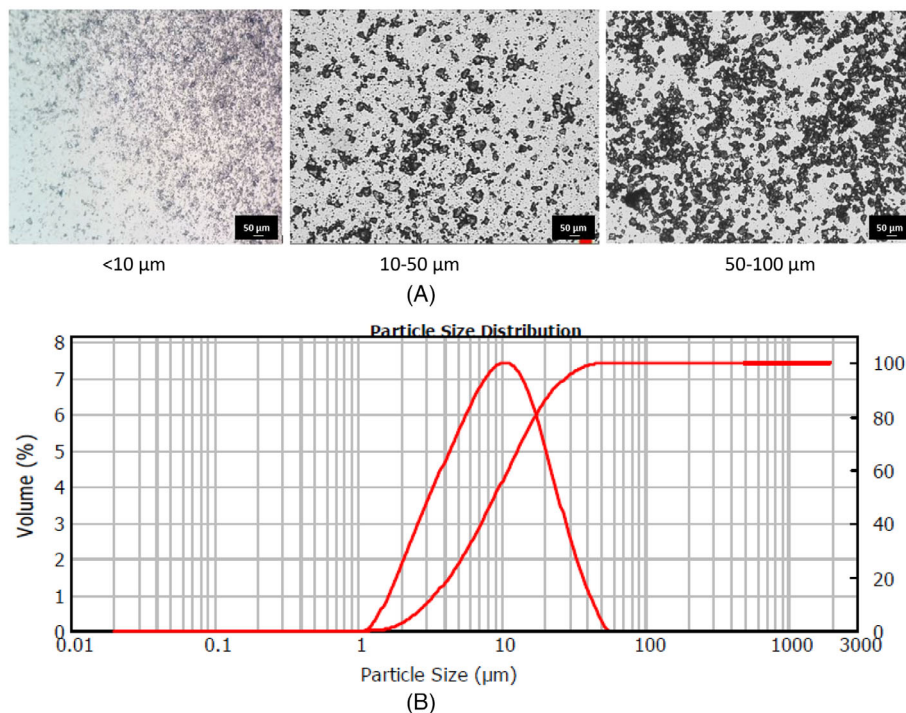
FIGURE 6 The size distribution of produced glass microparticles is as follows: (A) Glass microparticle size distribution and homogeneity under a microscope. (B) Size distribution analysis of particles with <10 μm size using a particle size analyzer. The bell curve in (B) depicts the relative distribution of particle sizes, indicating that the mean size of the particles is approximately 10 μm. The sigmoid curve represents the cumulative volume of the particles, showing that 100% of the particles are smaller than 52 μm in size.

the supernatant when an insufficient volume was present at the focal point. Conversely, increasing the droplet volume resulted in longer lysis times, as supported by both modeling and experimental results.

The size of glass microparticles emerged as a crucial factor influencing cell lysis efficiency in this study. Both the model and practical analysis revealed that only combinations with particle sizes <10 μm achieved high-efficiency lysis (close to 100%). When particles were used at low concentrations (1–2 μg/mL), no significant difference in lysis efficiency was observed. However, higher concentrations of particles could saturate the droplets and interfere with the efficient velocity required for lysis.

Lysis time was identified as another critical factor impacting lysis efficiency, with longer processing times resulting in higher efficiency (p-value <0.0001). In this device, almost all cells were lysed within a maximum of 5 min, which is acceptable for most POC applications.

Recent studies have introduced surface acoustic wave (SAW)-based methods for cell or exosome lysis [17, 33, 34]. However, these new SAW lysis methods face challenges such as low lysis efficiency and high-energy loss. To enhance lysis efficiency, several studies have integrated SAW-based methods with bead milling, where particle concentration, size, stream velocity, and time are crucial elements contributing to shear stress levels and efficient cell lysis [6, 35].

The current design of the acoustofluidic lysis device utilizes sharp-edge particles instead of beads, which create local high-shear zones when engaged by the transducer at −20 dBm, inducing an acoustic streaming effect. Increasing the driving energy of the transducer significantly amplifies the streaming velocity. Experimental results clearly indicate the significance of particle size and lysis time in the device's lysis efficiency (p-value <0.0001). Reducing particle size has been shown to enhance cell lysis efficiency. While several factors can impact lysis efficiency, the mean value demonstrates notable distinctions, particularly when considering particle size in isolation. To illustrate, when the particle size is ≤10 μm, the lysis efficiency reaches 0.40. In contrast, larger particle sizes, specifically 10–50 μm, 50–100 μm, and 100–150 μm, result in a significant portion of intact cells, exhibiting lysis efficiencies of 0.35, 0.31, and 0.1, respectively. Conversely, the presence of microparticles with a size of ≤10 μm yields a substantial amount of cell debris, as depicted in Figure 7.

The size and shape of beads or microparticles play a critical role in SAW-based cell lysis methods. Studies [15, 32] have demonstrated that microparticle diameter is a crucial parameter in the SAW-bead milling integrated cell lysis method. The momentum difference between target cells and microparticles plays a vital role in generating higher shearing forces. If the microparticle size exceeds that of the target cells, it is unlikely to generate higher velocities
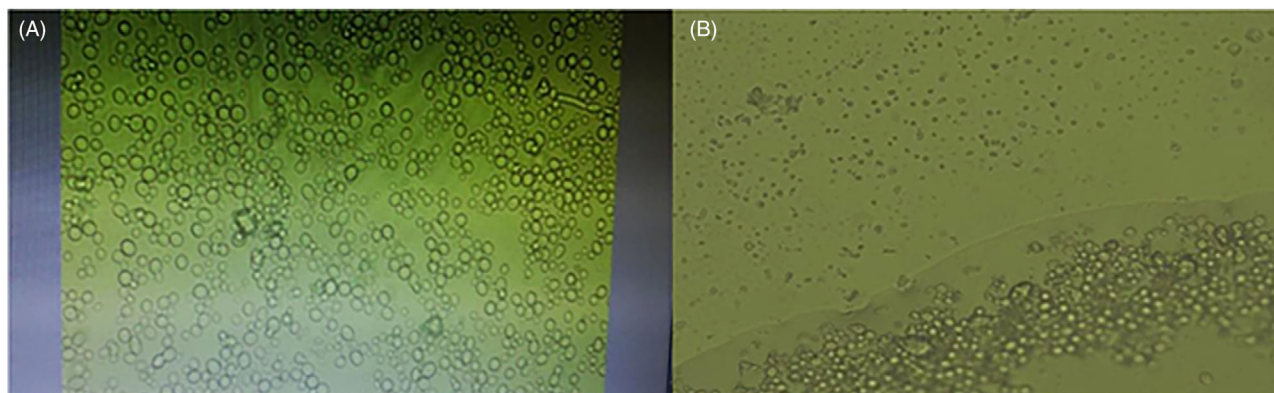
FIGURE 7 Acoustic-wave based cell lysis results. (A) *Candida albicans* strain SC 5314 cell line be-fore lysis. (B) *Candida albicans* strain SC 5314 cell line after 5 min acoustic-wave based lysis with 10 μm glass particles. Cell lysate (B) upper side versus cell-particle suspension (B) bottom side.

than the cells. Conversely, very small particles result in similar velocities to the cells within the droplet, thereby decreasing cell lysis efficiency within a greater particle size range. Optimal momentum conditions occur when cells and microparticles spin together in a rotating flow, allowing continuous exposure of the cells to shear forces, contributing to higher efficiency. Therefore, the decrease in cell lysis efficiency for larger particle sizes in the current study can be explained by the decrease in momentum differences.

4.3 | Analysis of cell lysate

The acoustofluidic device developed in this study operates based on mechanical forces, particularly shear forces, to disrupt cells. This unique approach enables the release of intracellular components in their native forms, eliminating the need for additional post-lysis procedures such as washing or purification. The downstream analysis conducted demonstrated the direct amplification of the target fragment from the lysate, as evidenced by the fluorescence levels and DNA concentrations presented in Table 2. This finding was further supported by the observed turbidity of the reaction sample and the results of the strip test, as illustrated in Figure 8. Collectively, these findings indicate the potential integration of the acoustofluidic lysis device into monolithic POC platforms.

4.4 | Comparison of characteristics and performance

The microchip-based cell lysis methods offer advantages such as precise control of fluid at micro and picoliter scales, single-cell analysis capabilities, and integration

with other microfluidic functions. These methods are suitable for various applications, including POC diagnostics, single-cell analysis, and high-throughput screening. Conventional lysis methods, on the other hand, may have limitations in terms of scalability, sample volume, and integration with other functions. However, they are often more established, cost-effective, and compatible with existing laboratory workflows (Table 3). The choice of lysis method depends on the specific application requirements, such as the sample type, target analyte, throughput, and available resources [14, 36–38].

Microchip cell lysis methods encompass a range of approaches, each with its own set of advantages and considerations. Chemical lysis relies on chemical agents to efficiently disrupt cell membranes and extract intracellular contents, but it may not be suitable for sensitive samples due to the harsh conditions it entails. Mechanical lysis, which involves physical methods like sonication or bead beating, is highly efficient but can introduce sample contamination and necessitate additional separation

TABLE 2 Fluorescent emission intensity and concentration of isothermal amplification products.

Samples	Fluorescent emission intensity RFU	Concentration (ng/μL)
Sample no 1	829859	5,44
Sample no 2	816484	5,32
Sample no 3	834113	5,26
Sample no 4	845751	5,78
Sample no 5	850429	5,77
Sample no 6	856327	5,77
Negative 1	333337	1,71
Negative 2	319776	1,69

TABLE 3 Comparing characteristics and performance of conventional versus microchip-based cell lysis methods.

Criteria	Conventional cell lysis		Microchip-based cell lysis				
	Mechanical	Chemical	Mechanical	Thermal	Laser	Electroporation	Acoustic
Efficiency	++	+	++	++	+++	+++	+++
Lysis time	+++	+++	++	++	+	++	+
Cost	++	+	+	++	+++	++	++
Sample size	+++	+++	+	+	+	+	+
Automation	+	+	+++	++	++	++	+++
Yield	++	+	+++	++	+++	+++	+++
Technical difficulty	++	+	++	++	+++	+++	+++
Potential of POC application	+	+	+++	+++	+++	+++	+++
Integration	+	+	+++	+++	+++	+++	+++

The table shows the evaluation of various criteria, such as efficiency, lysis time, cost, sample size, automation, yield, technical difficulty, potential of point-of-care application, and integration of multiple functions [14, 43]. The table uses a scale of + (low), ++ (medium), and +++ (high) to indicate the level of each criterion for each method.

steps. Electrical methods employ electric fields for gentle and efficient cell membrane disruption, yet they demand specialized equipment and may not universally accommodate all cell types. Laser lysis, while precise and ideal for single-cell analysis, comes with a higher cost and complexity in setup. Thermal lysis relies on temperature variations to rupture cell membranes, offering simplicity and cost-effectiveness, though it may not be universally applicable [14, 21].

FIGURE 8 Results of direct Loop-mediated isotherm amplification from the cell lysate. The reaction fluid white turbidity in daylight and detection of amplicons labeled with biotin and fluorescein isothiocyanate via lateral flow test. 1−2: Cell-free Phosphate-buffered saline was used as negative control, 3−8: *Candida albicans* cells lysate.

In contrast, the Surface Acoustic Wave (SAW) method, hinging on guided waves along a material's top surface with orthogonal wave vectors, presents a compelling alternative. SAW-based cell lysis exhibits remarkable efficiency, catering to various cell types, including bacteria and mammalian cells. Its mechanism allows for gentle cell membrane deformation, facilitating lysis. Speed is a notable asset, with SAW-based lysis occurring swiftly within seconds to minutes. Moreover, the SAW method adapts seamlessly to diverse sample volumes, from nanoliter droplets to larger microfluidic channels. While implementation costs may vary depending on specific equipment and applications, SAW technology holds promise for cost-effective integration into lab-on-a-chip devices [17, 21, 39–42].
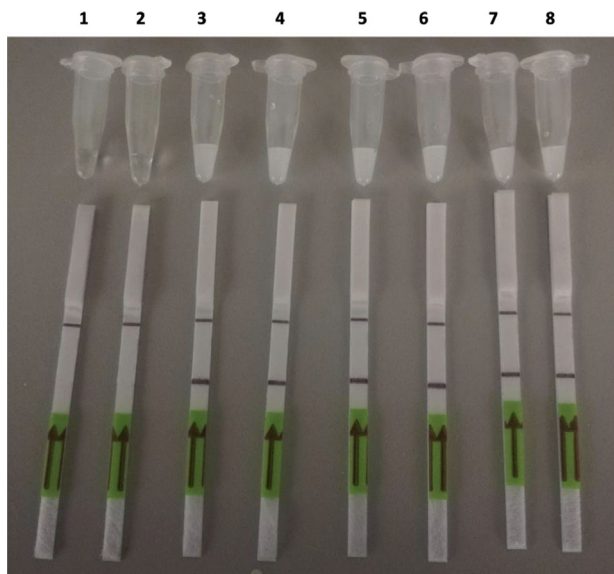
5 | CONCLUSIONS

The present study introduces an innovative acoustofluidic device designed for cell lysis, utilizing acoustic streaming-induced collisions between cells and microparticles. Through systematic experimentation, the optimal conditions for achieving effective cell lysis were determined to include a particle size of ≤10 μm, a concentration of 0.1 μg/mL, a lysis time of 5 min, a sample volume of 20 μL, and an input power of 2.5 W to generate surface acoustic waves (SAW) at the resonance frequency of 15.484 MHz. Notably, downstream analysis revealed that the lysis products obtained from this process can be directly utilized for subsequent analysis without requiring additional purification steps. These findings present a promising avenue for the development of monolithic POC platforms specifically tailored for rapid isothermal amplification techniques.

ORCID

Abbas Ali Husseini https://orcid.org/0000-0002-8861-7106

REFERENCES

1. Wei X, Li J, Wang L, Yang F. Low-voltage electrical cell lysis using a microfluidic device. *Biomed Microdevices*. 2019;21:22.
2. Brown RB, Audet J. Current techniques for single-cell lysis. *J R Soc Interface*. 2008;5:131.
3. Shehadul Islam M, Aryasomayajula A, Selvaganapathy P. A review on macroscale and microscale cell lysis methods. *Micromachines (Basel)*. 2017;8:83.
4. Levy R, Okun Z, Shpigelman A. High-pressure homogenization: principles and applications beyond microbial inactivation. *Food Eng Rev*. 2021;13:490-508.
5. Husseini AA, Derakhshandeh M, Tatlisu NB. Comprehensive review of transcriptomics (RNAs) workflows from blood specimens. *Sep Purif Rev*. 2022;51:57-77.
6. Salehi-Reyhani A, Gesellchen F, Mampallil D, et al. Chemical-free lysis and fractionation of cells by use of surface acoustic waves for sensitive protein assays. *Anal Chem*. 2015;87:2161-2169.
7. Kim J, Johnson M, Hill P, Gale BK. Microfluidic sample preparation: cell lysis and nucleic acid purification. *Integr Biol*. 2009;1:574-586.
8. Mauk MG, Liu C, Sadik M, Bau HH. Microfluidic devices for nucleic acid (NA) isolation, isothermal NA amplification, and real-time detection. *Methods Mol Biol*. 2015;1256:15-40.
9. Wang Z, Zhe J. Recent advances in particle and droplet manipulation for lab-on-a-chip devices based on surface acoustic waves. *Lab Chip*. 2011;11:1280.
10. Jahromi AK, Saadatmand M, Eghbal M, Yeganeh LP. Development of simple and efficient Lab-on-a-Disc platforms for automated chemical cell lysis. *Sci Rep*. 2020;10:11039.
11. Lim D, Yoo JC. Chemical cell lysis system applicable to lab-on-a-disc. *Appl Biochem Biotechnol*. 2017;183:20-29.
12. Seo M-J, Yoo J-C. Lab-on-a-disc platform for automated chemical cell lysis. *Sensors*. 2018;18:687.
13. Ding X, Li P, Lin S-CS, et al. Surface acoustic wave microfluidics. *Lab Chip*. 2013;13:3626.
14. Grigorov E, Kirov B, Marinov MB, Galabov V. Review of microfluidic methods for cellular lysis. *Micromachines (Basel)*. 2021;12:498.
15. Mutafopulos K, Lu PJ, Garry R, et al. Selective cell encapsulation, lysis, pico-injection and size-controlled droplet generation using traveling surface acoustic waves in a microfluidic device. *Lab Chip*. 2020;20:3914-3921.
16. Lu H, Mutafopulos K, Heyman JA, et al. Rapid additive-free bacteria lysis using traveling surface acoustic waves in microfluidic channels. *Lab Chip*. 2019;19:4064-4070.
17. Lyford TJ, Millard PJ, da Cunha MP. Cell Lysis using surface acoustic wave devices for sensor applications. In: *2012 IEEE International Ultrasonics Symposium*, 2012, pp. 1216-1219.
18. Wang W, Chen Y, Farooq U, et al. Ultrafast chemical-free cell lysis by high speed stream collision induced by surface acoustic waves. *Appl Phys Lett*. 2017;110:143504.
19. APITech, SAW Technology. https://Info.Apitech.Com/Saw-Technology-Va (accessed: December 2023)
20. Gedge M, Hill M. Acoustofluidics 17: theory and applications of surface acoustic wave devices for particle manipulation. *Lab Chip*. 2012;12:2998.
21. Ding X, Li P, Lin S-CS, et al. Surface acoustic wave microfluidics. *Lab Chip*. 2013;13:3626-3649.
22. Tan MK, Friend JR, Yeo LY. Direct visualization of surface acoustic waves along substrates using smoke particles. *Appl Phys Lett*. 2007;91:224101.
23. Delsing P, Cleland AN, Schuetz MJA, et al. The 2019 surface acoustic waves roadmap. *J Phys D Appl Phys*. 2019;52:353001.
24. Crampin S, Seismology Q. Theory and methods, Volumes I and II by Keiiti Aki and Paul G. Richards. W. H. Freeman and Co., San Francisco. Price: £41·40. *Geol J*. 2007;16:90-90.
25. Yang C-G, Xu Z-R, Wang J-H. Manipulation of droplets in microfluidic systems. *TrAC, Trends Anal Chem*. 2010;29:141-157.
26. Destgeer G, Ha BH, Park J, et al. Travelling surface acoustic waves microfluidics. *Phys Procedia*. 2015;70:34-37.
27. Bruus H. Acoustofluidics 7: the acoustic radiation force on small particles. *Lab Chip*. 2012;12:1014-1021.
28. Nama N, Barnkob R, Mao Z, et al. Numerical study of acoustophoretic motion of particles in a PDMS microchannel driven by surface acoustic waves. *Lab Chip*. 2015;15:2700-2709.
29. Frommelt T, Gogel D, Kostur M, et al. Flow patterns and transport in Rayleigh surface acoustic wave streaming: combined finite element method and raytracing numerics versus experiments. *IEEE Trans Ultrason Ferroelectr Freq Control*. 2008;55:2298-2305.

30. Yazdani AM. Size based micro particle separation using a novel acoustophoresis based microfluidic system, Marmara University, 2019.

31. Yazdani AM, Şişman A. A novel numerical model to simulate acoustofluidic particle manipulation. *Phys Scr.* 2020;95:95002.

32. Reboud J, Bourquin Y, Wilson R, et al. Shaping acoustic fields as a toolset for microfluidic manipulations in diagnostic technologies. *Proc Natl Acad Sci.* 2012;109:15162-15167.

33. Taller D, Richards K, Slouka Z, et al. On-chip surface acoustic wave lysis and ion-exchange nanomembrane detection of exosomal RNA for pancreatic cancer study and diagnosis. *Lab Chip.* 2015;15:1656-1666.

34. Richards KE, Go DB, Hill R. Surface acoustic wave lysis and ion-exchange membrane quantification of exosomal MicroRNA. In: Dalmay T, ed. *MicroRNA detection and target identification: methods and protocols.* Springer New York; 2017: 5970.

35. Wang S, Lv X, Su Y, et al. Piezoelectric microchip for cell lysis through cell-microparticle collision within a microdroplet driven by surface acoustic wave oscillation. *Small.* 2019;15:1804593.

36. Scott SM, Ali Z. Fabrication methods for microfluidic devices: an overview. *Micromachines (Basel).* 2021;12:319.

37. Gorgannezhad L, Stratton H, Nguyen N-T. Microfluidic-based nucleic acid amplification systems in microbiology. *Micromachines (Basel).* 2019;10:408.

38. Jagannath A, Li Y, Cong H, et al. UV-assisted hyperbranched poly(β-amino ester) modification of a silica membrane for two-step microfluidic DNA extraction from blood. *ACS Appl Mater Interfaces.* 2023;15:31159-31172.

39. Wang S, Lv X. Piezoelectric microchip for cell lysis through cell–microparticle collision within a microdroplet driven by surface acoustic wave oscillation. *Small.* 2019;15:e1804593.

40. Huang Y, Das PK, Bhethanabotla VR. Surface acoustic waves in biosensing applications. *Sensors and Actuators Reports.* 2021;3:100041.

41. Mandal D, Banerjee S. Surface acoustic wave (SAW) sensors: physics, materials, and applications. *Sensors.* 2022;22:820.

42. Damhorst GL, Duarte-Guevara C, Chen W, et al. Smartphone-imaged HIV-1 Reverse-Transcription Loop-Mediated Isothermal Amplification (RT-LAMP) on a chip from whole blood. *Engineering.* 2015;1:324-335.

43. Nan L, Jiang Z, Wei X. Emerging microfluidic devices for cell lysis: a review. *Lab Chip.* 2014;14:1060-1073.

SUPPORTING INFORMATION

Additional supporting information can be found online in the Supporting Information section at the end of this article.